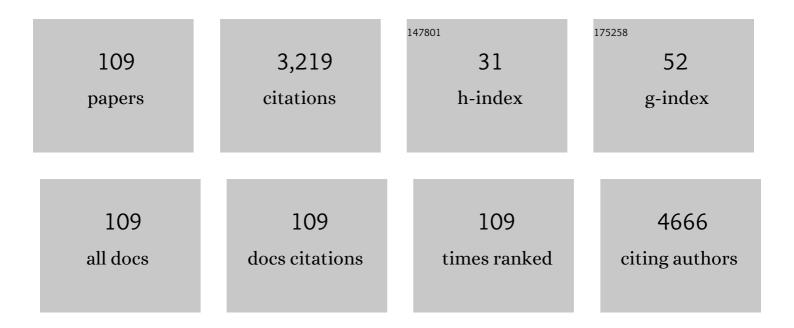


## List of Publications by Year in descending order

Source: https://exaly.com/author-pdf/480471/publications.pdf Version: 2024-02-01



LIE XIAO

#	Article	IF	CITATIONS
1	BM-RCGL: Benchmarking Approach for Localization of Reliability-Critical Gates in Combinational Logic Blocks. IEEE Transactions on Computers, 2022, 71, 1063-1076.	3.4	9
2	A novel Chinese parasol leaf biochar fuelled direct carbon solid oxide fuel cell for high performance electricity generation. International Journal of Hydrogen Energy, 2022, 47, 1172-1182.	7.1	16
3	Flower-like three-dimensional bifunctional cathode catalyst for high-performance Li–O2 batteries: ZIF-67@3D-N/rGO. Ceramics International, 2022, 48, 5601-5608.	4.8	5
4	Identifying Reliability-Critical Primary Inputs of Combinational Circuits Based on the Model of Gate-Sensitive Attributes. IEEE Transactions on Computer-Aided Design of Integrated Circuits and Systems, 2022, 41, 4708-4720.	2.7	6
5	Structural and functional biomarkers of the insula subregions predict sex differences in aggression subscales. Human Brain Mapping, 2022, 43, 2923-2935.	3.6	3
6	Accelerating stochasticâ€based reliability estimation for combinational circuits at RTL using GPU parallel computing. International Journal of Intelligent Systems, 2022, 37, 8309-8326.	5.7	1
7	Investigation on the formation mechanism of twinned crystals of hypoxanthine-doped beta-phase anhydrous guanine microplatelets. CrystEngComm, 2021, 23, 3444-3452.	2.6	7
8	Uniform non-Bernoulli sequences oriented locating method for reliability-critical gates. Tsinghua Science and Technology, 2021, 26, 24-35.	6.1	7
9	Stable Acidic Water Oxidation with a Cobalt–Iron–Lead Oxide Catalyst Operating via a Cobaltâ€Selective Selfâ€Healing Mechanism. Angewandte Chemie - International Edition, 2021, 60, 15821-15826.	13.8	23
10	Stable Acidic Water Oxidation with a Cobalt–Iron–Lead Oxide Catalyst Operating via a Cobaltâ€5elective Selfâ€Healing Mechanism. Angewandte Chemie, 2021, 133, 15955-15960.	2.0	3
11	Nafionâ€Induced Reduction of Manganese and its Impact on the Electrocatalytic Properties of a Highly Active MnFeNi Oxide for Bifunctional Oxygen Conversion**. ChemElectroChem, 2021, 8, 2979-2983.	3.4	13
12	Highly efficient utilization of industrial barium slag for carbon gasification in direct carbon solid oxide fuel cells. International Journal of Hydrogen Energy, 2021, 46, 37029-37038.	7.1	8
13	Sex-related Difference in Mental Rotation Performance is Mediated by the special Functional Connectivity Between the Default Mode and Salience Networks. Neuroscience, 2021, 478, 65-74.	2.3	5
14	A Microtubular Direct Carbon Solid Oxide Fuel Cell Operated on the Biochar Derived from Pepper Straw. Energy Technology, 2020, 8, 1901077.	3.8	18
15	In-Situ X-ray Spectroscopy of the Electric Double Layer around TiO <sub>2</sub> Nanoparticles Dispersed in Aqueous Solution: Implications for H <sub>2</sub> Generation. ACS Applied Nano Materials, 2020, 3, 264-273.	5.0	15
16	Performance improvement of a direct carbon solid oxide fuel cell via strontium-catalyzed carbon gasification. International Journal of Hydrogen Energy, 2020, 45, 23368-23377.	7.1	14
17	Facile synthesis of cobalt nanoparticles encapsulated in nitrogen-doped carbon nanotubes for use as a highly efficient bifunctional catalyst in rechargeable Zn-Air batteries. Journal of Alloys and Compounds, 2020, 842, 155791.	5.5	16
18	Blends based P(VDF-CTFE) with quenching in ice water and PLZST modification with high energy storage performance. Polymer, 2020, 202, 122727.	3.8	4

**JIE ΧΙΑΟ** 

#	Article	IF	CITATIONS
19	Improving Robustness of Interdependent Networks by Reducing Key Unbalanced Dependency Links. IEEE Transactions on Circuits and Systems II: Express Briefs, 2020, 67, 3187-3191.	3.0	9
20	Characterization of the soft X-ray spectrometer PEAXIS at BESSYâ€II. Journal of Synchrotron Radiation, 2020, 27, 238-249.	2.4	23
21	A Stochastic-Based Reliability Calculation Method for RTL Circuits. , 2020, , .		0
22	Facile design of ultrafine CuFe2O4 nanocrystallines coupled porous carbon nanowires: Highly effective electrocatalysts for hydrogen peroxide reduction and the oxygen evolution reaction. Journal of Alloys and Compounds, 2019, 809, 151766.	5.5	36
23	Effect of pre-calcined ceramic powders at different temperatures on Ni-YSZ anode-supported SOFC cell/stack by low pressure injection molding. Ceramics International, 2019, 45, 20066-20072.	4.8	23
24	A novel strategy for realizing high nitrogen doping in Fe <sub>3</sub> C-embedded nitrogen and phosphorus-co-doped porous carbon nanowires: efficient oxygen reduction reaction catalysis in acidic electrolytes. Journal of Materials Chemistry A, 2019, 7, 17923-17936.	10.3	47
25	Circuit reliability prediction based on deep autoencoder network. Neurocomputing, 2019, 370, 140-154.	5.9	5
26	New insights into carbon deposition mechanism of nickel/yttrium-stabilized zirconia cermet from methane by in situ investigation. Applied Energy, 2019, 256, 113910.	10.1	24
27	Comparative Study of Yttria-Stabilized Zirconia Synthesis by Co-Precipitation and Solvothermal Methods. Jom, 2019, 71, 3806-3813.	1.9	7
28	Low Remanent Polarization for High Energy Density by Poly(vinylidene) Tj ETQq0 0 0 rgBT /Overlock 10 Tf 50 387 Materials, 2019, 48, 8172-8180.	Td (fluoric 2.2	le-co-chlorc 4
29	A Locating Method for Reliability-Critical Gates with a Parallel-Structured Genetic Algorithm. Journal of Computer Science and Technology, 2019, 34, 1136-1151.	1.5	8
30	Evolution of Oxygen–Metal Electron Transfer and Metal Electronic States During Manganese Oxide Catalyzed Water Oxidation Revealed with Inâ€Situ Soft Xâ€Ray Spectroscopy. Angewandte Chemie, 2019, 131, 3464-3470.	2.0	28
31	Influence of surface chemistry on optical, chemical and electronic properties of blue luminescent carbon dots. Nanoscale, 2019, 11, 2056-2064.	5.6	94
32	Uncovering the Charge Transfer between Carbon Dots and Water by In Situ Soft X-ray Absorption Spectroscopy. Journal of Physical Chemistry Letters, 2019, 10, 3843-3848.	4.6	13
33	A high performance direct carbon solid oxide fuel cell – A green pathway for brown coal utilization. Applied Energy, 2019, 248, 679-687.	10.1	74
34	Generalized Synchronization Between Chen System and Rucklidge System. IEEE Access, 2019, 7, 8519-8526.	4.2	11
35	A Fast and Effective Sensitivity Calculation Method for Circuit Input Vectors. IEEE Transactions on Reliability, 2019, 68, 938-953.	4.6	14
36	Evolution of Oxygen–Metal Electron Transfer and Metal Electronic States During Manganese Oxide Catalyzed Water Oxidation Revealed with Inâ€Situ Soft Xâ€Ray Spectroscopy. Angewandte Chemie - International Edition, 2019, 58, 3426-3432.	13.8	52

**JIE ΧΙΑΟ** 

#	Article	IF	CITATIONS
37	Blockchain Architecture Reliability-Based Measurement for Circuit Unit Importance. IEEE Access, 2018, 6, 15326-15334.	4.2	9
38	Enhanced electrokinetic remediation of lead- and cadmium-contaminated paddy soil by composite electrolyte of sodium chloride and citric acid. Journal of Soils and Sediments, 2018, 18, 1915-1924.	3.0	40
39	Co-precipitation synthesis of alumina doped yttria stabilized zirconia. Journal of Alloys and Compounds, 2018, 731, 1080-1088.	5.5	22
40	Honeycomb-like Hard Carbon Derived from Pine Pollen as High-Performance Anode Material for Sodium-Ion Batteries. ACS Applied Materials & Interfaces, 2018, 10, 42796-42803.	8.0	129
41	Link prediction based on local major path degree. Modern Physics Letters B, 2018, 32, 1850348.	1.9	7
42	Laplacian Centrality Peaks Clustering Based on Potential Entropy. IEEE Access, 2018, 6, 55462-55472.	4.2	1
43	Effective and environmentally friendly recycling process designed for LiCoO2 cathode powders of spent Li-ion batteries using mixture of mild organic acids. Waste Management, 2018, 78, 51-57.	7.4	55
44	A Novel Trust Evaluation Method for Logic Circuits in IoT Applications Based on the E-PTM Model. IEEE Access, 2018, 6, 35683-35696.	4.2	6
45	Innovative Savonius rotors evolved by genetic algorithm based on 2D-DCT encoding. Soft Computing, 2018, 22, 8001-8010.	3.6	10
46	Thermal-aware SoC Test Scheduling with Voltage/Frequency Scaling and Test Partition. Journal of Electronic Testing: Theory and Applications (JETTA), 2018, 34, 447-460.	1.2	1
47	Insight into pHâ€Dependent Formation of Manganese Oxide Phases in Electrodeposited Catalytic Films Probed by Soft Xâ€Ray Absorption Spectroscopy. ChemPlusChem, 2018, 83, 721-727.	2.8	5
48	Chemical bonding in aqueous hexacyano cobaltate from photon- and electron-detection perspectives. Scientific Reports, 2017, 7, 40811.	3.3	14
49	Multiscale Photo-Based In-Situ and Operando Spectroscopies in Time and Energy Landscapes. Synchrotron Radiation News, 2017, 30, 14-19.	0.8	2
50	TiO2–MoS2 hybrid nano composites with 3D network architecture as binder-free flexible electrodes for lithium ion batteries. Journal of Materials Science: Materials in Electronics, 2017, 28, 9519-9527.	2.2	21
51	In Situ L-Edge XAS Study of a Manganese Oxide Water Oxidation Catalyst. Journal of Physical Chemistry C, 2017, 121, 12003-12009.	3.1	40
52	Introducing Ionic-Current Detection for X-ray Absorption Spectroscopy in Liquid Cells. Journal of Physical Chemistry Letters, 2017, 8, 2087-2092.	4.6	16
53	Combustion synthesized macroporous structure MFe 2 O 4 (M= Zn, Co) as anode materials with excellent electrochemical performance for lithium ion batteries. Journal of Alloys and Compounds, 2017, 699, 401-407.	5.5	38
54	Bulk-Sensitive Detection of the Total Ion Yield for X-ray Absorption Spectroscopy in Liquid Cells. Journal of Physical Chemistry Letters, 2017, 8, 5136-5140.	4.6	10

**JIE ΧΙΑΟ** 

#	Article	lF	CITATIONS
55	IrO2 nanoparticles highly dispersed on nitrogen-doped carbon nanotubes as an efficient cathode catalyst for high-performance Li-O2 batteries. Ceramics International, 2017, 43, 14082-14089.	4.8	46
56	A Method of Gate-level Circuit Yield Calculation Based on PTM. Procedia Computer Science, 2017, 107, 674-684.	2.0	0
57	Xâ€Ray Absorption Spectroscopy of TiO <sub>2</sub> Nanoparticles in Water Using a Holey Membraneâ€Based Flow Cell. Advanced Materials Interfaces, 2017, 4, 1700755.	3.7	11
58	Effects of doping alumina on the electrical and sintering performances of yttrium-stabilized-zirconia. Solid State Ionics, 2016, 289, 28-34.	2.7	40
59	Circuit reliability estimation based on an iterative PTM model with hybrid coding. Microelectronics Journal, 2016, 52, 117-123.	2.0	12
60	An investigation on the kinetics of direct carbon solid oxide fuel cells. Journal of Solid State Electrochemistry, 2016, 20, 2207-2216.	2.5	34
61	Undistorted X-ray Absorption Spectroscopy Using s-Core-Orbital Emissions. Journal of Physical Chemistry A, 2016, 120, 2808-2814.	2.5	21
62	Characterization of symmetrical SrFe0.75Mo0.25O3â^`δ electrodes in direct carbon solid oxide fuel cells. Journal of Alloys and Compounds, 2016, 688, 939-945.	5.5	61
63	Analysis of the Electronic Structure of Aqueous Urea and Its Derivatives: A Systematic Soft Xâ€Ray–TDâ€DFT Approach. Chemistry - A European Journal, 2016, 22, 12040-12049.	3.3	6
64	Joint Analysis of Radiative and Non-Radiative Electronic Relaxation Upon X-ray Irradiation of Transition Metal Aqueous Solutions. Scientific Reports, 2016, 6, 24659.	3.3	38
65	Influence of the Outer Ligands on Metal-to-Ligand Charge Transfer in Solvated Manganese Porphyrins. Inorganic Chemistry, 2016, 55, 22-28.	4.0	10
66	Chemical Speciation and Bond Lengths of Organic Solutes by Core‣evel Spectroscopy: pH and Solvent Influence on <i>p</i> â€Aminobenzoic Acid. Chemistry - A European Journal, 2015, 21, 7256-7263.	3.3	15
67	Valence holes observed in nanodiamonds dispersed in water. Nanoscale, 2015, 7, 2987-2991.	5.6	33
68	Local Energy Gap Opening Induced by Hemin Dimerization in Aqueous Solution. Journal of Physical Chemistry B, 2015, 119, 3058-3062.	2.6	11
69	Electrolysis of Carbon Dioxide in a Solid Oxide Electrolyzer with Silver-Gadolinium-Doped Ceria Cathode. Journal of the Electrochemical Society, 2015, 162, F397-F402.	2.9	47
70	Enhancing Catalytic Activity by Narrowing Local Energy Gaps—Xâ€Ray Studies of a Manganese Water Oxidation Catalyst. ChemSusChem, 2015, 8, 872-877.	6.8	7
71	Unraveling the Electronic Structure of Photocatalytic Manganese Complexes by L-Edge X-ray Spectroscopy. Journal of Physical Chemistry C, 2015, 119, 19192-19200.	3.1	40
72	On the Origin of the Improvement of Electrodeposited MnOxFilms in Water Oxidation Catalysis Induced by Heat Treatment. ChemSusChem, 2015, 8, 1980-1985.	6.8	20

**JIE XIAO** 

#	Article	IF	CITATIONS
73	Intermolecular bonding of hemin in solution and in solid state probed by N K-edge X-ray spectroscopies. Physical Chemistry Chemical Physics, 2015, 17, 29000-29006.	2.8	9
74	Co(iii) protoporphyrin IX chloride in solution: spin-state and metal coordination revealed from resonant inelastic X-ray scattering and electronic structure calculations. Physical Chemistry Chemical Physics, 2015, 17, 3409-3414.	2.8	12
75	Electrochemical gas–electricity cogeneration through direct carbon solid oxide fuel cells. Journal of Power Sources, 2015, 277, 1-8.	7.8	52
76	Coverage―and Temperatureâ€Dependent Metalation and Dehydrogenation of Tetraphenylporphyrin on Cu(111). Chemistry - A European Journal, 2014, 20, 8948-8953.	3.3	19
77	Behavior of strontium- and magnesium-doped gallate electrolyte in direct carbon solid oxide fuel cells. Journal of Alloys and Compounds, 2014, 608, 272-277.	5.5	40
78	Abrupt Coverage-Induced Enhancement of the Self-Metalation of Tetraphenylporphyrin with Cu(111). Journal of Physical Chemistry C, 2014, 118, 1661-1667.	3.1	51
79	Coordination Reactions and Layer Exchange Processes at a Buried Metal–Organic Interface. Journal of Physical Chemistry C, 2014, 118, 8501-8507.	3.1	19
80	Electronic Structure of Hemin in Solution Studied by Resonant X-ray Emission Spectroscopy and Electronic Structure Calculations. Journal of Physical Chemistry B, 2014, 118, 9938-9943.	2.6	16
81	Deactivation of nickel-based anode in solid oxide fuel cells operated on carbon-containing fuels. Journal of Power Sources, 2014, 268, 508-516.	7.8	66
82	Assistance of the Iron Porphyrin Ligands to the Binding Interaction between the Fe Center and Small Molecules in Solution. Journal of Physical Chemistry B, 2014, 118, 9371-9377.	2.6	7
83	Combined Photoemission and Scanning Tunneling Microscopy Study of the Surface-Assisted Ullmann Coupling Reaction. Journal of Physical Chemistry C, 2014, 118, 6820-6830.	3.1	84
84	Wet Chemical Synthesis of Graphene. Advanced Materials, 2013, 25, 3583-3587.	21.0	453
85	Coordination and Metalation Bifunctionality of Cu with 5,10,15,20-Tetra(4-pyridyl)porphyrin: Toward a Mixed-Valence Two-Dimensional Coordination Network. Journal of the American Chemical Society, 2012, 134, 6401-6408.	13.7	199
86	Altering the Static Dipole on Surfaces through Chemistry: Molecular Films of Zwitterionic Quinonoids. Journal of the American Chemical Society, 2012, 134, 8494-8506.	13.7	37
87	Surface state engineering of molecule–molecule interactions. Physical Chemistry Chemical Physics, 2012, 14, 4971.	2.8	56
88	Temperature-Dependent Chemical and Structural Transformations from 2H-tetraphenylporphyrin to Copper(II)-Tetraphenylporphyrin on Cu(111). Journal of Physical Chemistry C, 2012, 116, 12275-12282.	3.1	68
89	Weak screening of a large dipolar molecule adsorbed on graphene. Carbon, 2012, 50, 1981-1986.	10.3	16
90	A Method of Gate-Level Circuit Reliability Estimation Based on Iterative PTM Model. , 2011, , .		8

A Method of Gate-Level Circuit Reliability Estimation Based on Iterative PTM Model. , 2011, , . 90

**Jie Χιαο** 

#	Article	IF	CITATIONS
91	Diffusion, Rotation, and Surface Chemical Bond of Individual 2 <i>H</i> -Tetraphenylporphyrin Molecules on Cu(111). Journal of Physical Chemistry C, 2011, 115, 24172-24177.	3.1	74
92	Surface charging at the (100) surface of Cu doped and undoped Li2B4O7. Applied Surface Science, 2011, 257, 3399-3403.	6.1	9
93	Electrochemical Performance of Cone-Shaped Tubular Anode Supported Solid Oxide Fuel Cells Fabricated by Low-Pressure Injection Moulding Technique. ECS Transactions, 2011, 35, 609-614.	0.5	2
94	The off-axis pyroelectric effect observed for lithium tetraborate. Physics Letters, Section A: General, Atomic and Solid State Physics, 2010, 374, 891-895.	2.1	18
95	The surface core level shift for lithium at the surface of lithium borate. Physica B: Condensed Matter, 2010, 405, 461-464.	2.7	13
96	The Electronic Structure and Secondary Pyroelectric Properties of Lithium Tetraborate. Materials, 2010, 3, 4550-4579.	2.9	24
97	The interface bonding and orientation of a quinonoid zwitterion. Physical Chemistry Chemical Physics, 2010, 12, 10329.	2.8	30
98	Graphene/Substrate Charge Transfer Characterized by Inverse Photoelectron Spectroscopy. Journal of Physical Chemistry C, 2010, 114, 21618-21624.	3.1	61
99	Self-Assembly and Properties of Nonmetalated Tetraphenyl-Porphyrin on Metal Substrates. Journal of Physical Chemistry C, 2010, 114, 9408-9415.	3.1	101
100	Franckâ^'Condon Coupling in Anthracene Isomer Self-Assembled Layers and Symmetry Effects on the High Resolution Ultraviolet Photoemission Spectra. Journal of Physical Chemistry C, 2010, 114, 1015-1018.	3.1	3
101	Selective nanoshaving of self-assembled monolayers of 2-(4-pyridylethyl)triethoxysilane. Materials Letters, 2009, 63, 961-964.	2.6	20
102	Adsorbate/absorbate interactions with organic ferroelectric polymers. Journal of Electron Spectroscopy and Related Phenomena, 2009, 174, 10-21.	1.7	16
103	Haloform adsorption on crystalline copolymer films of vinylidene fluoride with trifluoroethylene. Surface Science, 2009, 603, 513-517.	1.9	4
104	The role of the interface in the electronic structure of adsorbed metal(II) (Co, Ni, Cu) phthalocyanines. Journal of Materials Chemistry, 2009, 19, 2172.	6.7	36
105	Electronic structure evidence for allâ€ŧrans poly(methylvinylidene cyanide). Polymer Engineering and Science, 2008, 48, 1649-1654.	3.1	4
106	Different approaches to adjusting band offsets at intermolecular interfaces. Applied Surface Science, 2008, 254, 4238-4244.	6.1	15
107	The Electronic Structures of Co and Ni Tetraazaannulenes. Journal of Physical Chemistry B, 2006, 110, 26180-26184.	2.6	10
108	Comparison of the electronic structure of two polymers with strong dipole ordering. Journal of Physics Condensed Matter, 2006, 18, L155-L161.	1.8	26

	JIE XI	40	
#	Article	IF	CITATIONS
109	Crystalline Ice Grown on the Surface of the Ferroelectric Polymer Poly(vinylidene fluoride) (70%) and Trifluoroethylene (30%). Journal of the American Chemical Society, 2005, 127, 17261-17265.	13.7	18